Commun. Theor. Phys. **66** (2016) 133–142 Vol. 66, No. 1, July 1, 2016

Mixed Convective Viscoelastic Nanofluid Flow Past a Porous Media with Soret–Dufour Effects

M. Ramzan,[1,*] Farhan Yousaf,[2] M. Farooq,[3] and Jae Dong Chung[4]

[1]Department of Computer Science, Bahria University, Islamabad Campus, Islamabad 44000, Pakistan
[2]Department of Mathematics, Faculty of Computing, Capital University of Science and Technology, Islamabad 44000, Pakistan
[3]Department of Mathematics, Riphah International University, Islamabad 44000, Pakistan
[4]Department of Mechanical Engineering, Sejong University, Seoul, 143-747, Korea

(Received March 14, 2016; revised manuscript received May 5, 2016)

Abstract *The present study is carried out to see the thermal-diffusion (Dufour) and diffusion-thermo (Soret) effects on the mixed convection boundary layer flow of viscoelastic nanofluid flow over a vertical stretching surface in a porous medium. Optimal homotopy analysis method (OHAM) is best candidate to handle highly nonlinear system of differential equations obtained from boundary layer partial differential equations via appropriate transformations. Graphical illustrations depicting different physical arising parameters against velocity, temperature and concentration distributions with required discussion have also been added. Numerically calculated values of skin friction coefficient, local Nusselt and Sherwood numbers are given in the form of table and well argued. It is found that nanofluid velocity increases with increase in mixed convective and viscoelastic parameters but it decreases with the increasing values of porosity parameter. Also, it is observed that Dufour number has opposite behavior on temperature and concentration profiles.*

PACS numbers: 47.15.Cb, 46.15.Ff
Key words: mixed convection, porous media, nanofluid flow, soret-dufour effects

1 Introduction

Heat transportation through a porous medium has been a subject of interest due to its numerous industrial applications including chemical catalytic reactors, high performance insulation for buildings, movement of moisture via air stringy insulations, packed sphere beds, grain storage, in/out of heat between soil and surrounding, discharge of salt from soil, electrochemical processes, solar power collectors, insulation of nuclear reactors, geothermal energy systems and regenerative heat exchangers, etc. Many interesting studies may be found in the literature. Highlighting some of these may include books by Ingham and Pop,[1] Nield and Bejan,[2] Pop and Ingham,[3] Bejan *et al.*,[4] Vafai,[5] Vadasz[6] and Jansen and Dirk,[7] etc.

In double-diffusive (e.g. thermohaline) convection, the dependency of fluid's mixture density on temperature and concentration results in coupling of heat and mass transfer. As stated by Nield and Bejan,[1] this mixture density linearly depends on temperature and concentration for suitably miniature isobaric changes in temperature and concentration. In a number of situations when there is a direct coupling between temperature and concentration, the effects of cross-diffusion (Soret and Dufour) cannot be ignored. In 1873, Dufour highlighted that composition gradient results in energy flux. This phenomenon is known as Dufour effect. However mass flux is an outcome of temperature gradient. This effect is found by Soret and is also named as thermo-diffusion effect. Postelnicu[8] found that soret effect is very useful in separation of isotopes and in mixture of gases with low (H_2, He) and medium (H_2, air) molecular weights. Effects of Soret and Dufour are neglected in many cases as their order of magnitude is smaller than those of Fourier's and Fick's laws. Nevertheless, exceptions can be considered. There are cases where effects of Soret and Dufour cannot be ignored as mentioned by Eckert and Drake.[9] Platten and Legros[10] explored that Soret and Dufour effects are inoperative in most liquid mixtures but in gases this law may not hold. In liquids the order of magnitude of Soret effect's coefficient is greater than that of Dufour effect. This fact is stated by Mojtabi and Charrier–Mojtabi.[11] Ramzan *et al.*[12] discussed collective consequences of Soret and Dufour in magnetohydrodynamics stagnation point flow by a permeable stretching cylinder. They concluded that by increasing Dufour and Soret numbers, temperature and concentration distributions show opposite behavior. Convective three-dimensional flow of Maxwell fluid with Soret and Dufour effects and chemical reaction is studied by Hayat *et al.*[13] They found that Soret and Dufour numbers depict contradictory approach with increasing values of temperature profile.

Boundary layer flows over stretched or moving surfaces are quite important in many industrial and metallurgical processes. In particular, it contains paper man-

*Corresponding author, E-mail: mramzan@bahria.edu.pk

ufacturing, glass-fiber, spinning of laments, unremitting casting, rolling of hot sheets, crystal growing, cooling of metal sheets or microelectronic chips, polymer in melting form, preservation and/or aeration of paper and textiles etc. Numerous investigations including numerical and analytical studies highlighting different features can be seen in (Ramzan and Farhan,[14] Shehzad *et al.*,[15] Makinde and Aziz,[16] Malvandi *et al.*,[17] Cortell,[18] Ramzan and Bilal,[19] Hayat *et al.*[20])

The miniaturization and efficiency of electronic devices is need of today's era as far as their perfection and meticulousness is concerned. The exigent chore in manufacturing these gadgets is their thermal performance. For instance, in different engineering processes, ordinary base fluid does not fulfill required cooling parameters. The introduction of nanofluids has triumph this complexity and transfigured the present industrial world with improved thermal conductivity of the base fluid. Choi's[21] coined work invited the follower researchers to dig out more novel ideas and has given a sound footing to the whole manufacturing industry with practical applications, which include food processing industry and automotives, fuel cells, hybrid-powered engines, pharmaceutical applications, refrigeration, chemical production, microelectronics cooling, transportation, and many other applications. The cutting-edge effort of Choi has been extended by many scientist and researchers. For example Mushtaq *et al.*[22] presented numerical solution of three-dimensional viscoelastic flow past a nonlinear stretching sheet. Combination of RK method with shooting approach is employed to address highly nonlinear differential equations. Three-dimensional elastico-viscous nanofluid flow with magnetic field and chemical reaction effects is studied by Ramzan and Bilal.[23] They found series solutions for nonlinear differential equations by Homotopy Analysis method. Dhanai *et al.*[24] studied mixed convective nanofluid slip flow past an inclined cylinder with viscous dissipation. Fourth-order RKF method with shooting technique is employed to solve the said problem numerically. Sheikholeslami and Ganji[25] analyzed MHD three-dimensional nanofluid flow in a rotating system. Numerical solution employing Fourth-order Runge–Kutta method is obtained. Some more investigations in this regard may be referred in Refs. [26–29].

The pivotal point of this investigation is to study the effects of mixed convection and Soret–Dufour on the flow of an incompressible viscoelastic nanofluid flow past a porous media. Mixed convection, a combination of free and forced convection which occur because of significant temperature difference between wall and the ambient fluid. Mixed convection has a vital role when the buoyancy forces significantly disrupt the flow and the thermal fields. On other hand, Soret and Dufour effects are imperative for intermediate molecular weight gases in coupled heat and mass transfer in binary systems, frequently occur in chemical process engineering. Optimal Homotopy analysis method (OHAM) suggested by Liao[30] is used to obtain the desired analytical solution. Many other problems of heat transfer and fluid mechanics have been solved with the help of this popular method OHAM.[31−34] The concept presented here is totally novel and has not been discussed in the literature before. Illustrations highlighting effects of protuberant parameters on velocity, temperature and concentration transformations are presented and argued. Numerically calculated tabulated results of skin friction, local Nusselt and Sherwood numbers against prominent arising parameters are presented and pondered.

2 Mathematical Formulation

We assume here an incompressible, two-dimensional viscoelastic nanofluid flow with uniform ambient temperature T_∞ and uniform ambient concentration C_∞ about a stretching vertical surface with variable temperature and concentration $T_w(x)$, $C_w(x)$ respectively, through a porous medium. Effects of mixed convection and Soret and Dufour are also considered. Surface is stretched linearly with the velocity $u_w(x) = ax$, where a is a constant. Boussinseq's approximation for temperature and concentration gradient are assumed due to presence of buoyancy and density variation effects. In view of above specified assumptions, boundary layer equations of the said system are given by:

$$\frac{\partial u}{\partial x} + \frac{\partial v}{\partial y} = 0\,, \tag{1}$$

$$u\frac{\partial u}{\partial x} + v\frac{\partial u}{\partial y} = \upsilon\frac{\partial^2 u}{\partial y^2} + k_0\Big(u\frac{\partial^3 u}{\partial x \partial y^2} + \frac{\partial u}{\partial x}\frac{\partial^2 u}{\partial y^2} + \frac{\partial u}{\partial y}\frac{\partial^2 v}{\partial y^2} + v\frac{\partial^3 u}{\partial y^3}\Big) - \frac{\nu}{K}u + g[\beta_T(T - T_\infty) + \beta_C(C - C_\infty)]\,, \tag{2}$$

$$u\frac{\partial T}{\partial x} + v\frac{\partial T}{\partial y} = \alpha_m\frac{\partial^2 T}{\partial y^2} + \frac{D_e K_T}{C_s C_p}\frac{\partial^2 C}{\partial y^2} + \tau\Big[D_B\frac{\partial C}{\partial y}\frac{\partial T}{\partial y} + \frac{D_T}{T_\infty}\Big(\frac{\partial T}{\partial y}\Big)^2\Big]\,, \tag{3}$$

$$u\frac{\partial C}{\partial x} + v\frac{\partial C}{\partial y} = \frac{D_e K_T}{T_m}\frac{\partial^2 T}{\partial y^2} + D_B\frac{\partial^2 C}{\partial y^2} + \frac{D_T}{T_\infty}\frac{\partial^2 T}{\partial y^2}\,. \tag{4}$$

The appropriate boundary conditions are

$$\begin{aligned} &u = u_w(x) = ax\,, \quad v = 0\,,\\ &T = T_w(x) = T_\infty + bx\,,\\ &C = C_w(x) = C_\infty + cx \text{ at } y = 0\,,\\ &u \to 0, \quad \frac{\partial u}{\partial y} \to 0, \quad T \to T_\infty\,,\\ &C \to C_\infty \text{ as } y \to \infty\,, \end{aligned} \tag{5}$$

where u and v are velocity component along and normal to the plate in x and y direction respectively. Here, k_0, α_m, g, T, τ, D_T, and D_B are viscoelastic parameter, thermal diffusivity, acceleration due to the gravity, fluid temperature, ratio of effective heat capacity of the nanoparticle material to base fluid heat capacity, thermophoretic diffusion coefficient and Brownian motion coefficient. Moreover,

$a > 0, b$ and $c > 0$ are constants with $b > 0$, $T_w > T_\infty$ for heated plate and $b < 0$, $T_w < T_\infty$ for a cooled surface.

Defining

$$\psi = x\sqrt{a\nu}f(\eta), \quad \theta(\eta) = \frac{T - T_\infty}{T_w - T_\infty}\,,$$
$$\phi(\eta) = \frac{C - C_\infty}{C_w - C_\infty}, \quad \eta = \sqrt{\frac{a}{\nu}}y\,, \tag{6}$$

condition of Eq. (1) is automatically fulfilled whereas Eqs. (2) to (4) take the form

$$f''' + ff'' - f'^2 - K(ff^{iv} - 2f'f''' + f'^2) - \gamma f' + \lambda(\theta + N\phi) = 0\,, \tag{7}$$
$$\frac{1}{\Pr}\theta'' + f\theta' - \theta f' + \mathrm{Df}\phi'' + \mathrm{Nb}\theta'\phi' + \mathrm{Nt}\theta'^2 = 0\,, \tag{8}$$
$$\phi'' + \mathrm{PrLe}(f\phi' - \phi f') + \mathrm{SrLe}\theta'' + \frac{\mathrm{Nt}}{\mathrm{Nb}}\theta'' = 0\,, \tag{9}$$
$$f(0) = 0, \quad f'(0) = 1, \quad \theta(0) = 1\,,$$
$$\phi(0) = 1, \quad f'(\infty) \to 0\,, \tag{10}$$
$$\theta(\infty) \to 0, \quad \phi(\infty) \to 0\,,$$

with $K(\geqslant 0)$, $\mathrm{Le} = \alpha_m/D_e$, N, $\Pr = \nu/\alpha_m$, λ, γ, Df, Sr, Nt, and Nb are dimensionless viscoelastic parameter, Lewis number, constant dimensionless concentration buoyancy parameter, Prandtl number, dimensionless mixed convection parameter, dimensionless porosity parameter, Dufour number, Soret number, thermophoresis parameter and Brownian motion parameter respectively and are given by

$$\lambda = \frac{g\beta_{_T}b}{a^2} = \frac{g\beta_T(T_w - T_\infty)x^3/\upsilon^2}{u_w^2x^2/\upsilon^2} = \frac{\mathrm{Gr}_x}{\mathrm{Re}_x^2}\,,$$
$$K = \frac{k_0a}{\nu}, \quad \gamma = \frac{\nu}{aK}, \quad N = \frac{\beta_C(C_w - C_\infty)}{\beta_T(T_w - T_\infty)}\,,$$
$$\mathrm{Df} = \frac{D_eK_T(C_w - C_\infty)}{C_sC_p(T_w - T_\infty)\upsilon}, \quad \mathrm{Sr} = \frac{D_eK_T(T_w - T_\infty)}{T_m\alpha_m(C_w - C_\infty)}\,,$$
$$\mathrm{Nb} = \frac{\tau D_B(C_w - C_\infty)}{\nu}, \quad \mathrm{Nt} = \frac{\tau D_T(T_w - T_\infty)}{T_\infty\nu}\,, \tag{11}$$

where Gr_x and $\mathrm{Re}_x = u_wx/\nu$ are local Grashof and local Reynolds numbers respectively. Here, $\lambda = 0$ for forced convection flow, $\lambda < 0$ relates to opposing flow (cooled plate) and $\lambda > 0$ corresponds to assisting flow (heated plate).

Skin friction coefficient (C_f), the local Nusselt (Nu_x) and the Sherwood (Sh) numbers are given by

$$C_f = \frac{\tau_w}{\rho u_w^2/2}, \quad \mathrm{Nu}_x = \frac{xq_w}{k(T_w - T_\infty)}\,,$$
$$\mathrm{Sh} = \frac{xj_w}{D_B(T_w - T_\infty)}\,, \tag{12}$$

where τ_w is wall skin friction, q_w is wall heat flux, and j_w is mass flux from the plate. These are given by

$$\tau_w = \mu\Big(\frac{\partial u}{\partial y}\Big)_{y=0} + k_0\Big(u\frac{\partial^2 u}{\partial x\partial y} + v\frac{\partial^2 u}{\partial y^2} - 2\frac{\partial v}{\partial y}\frac{\partial u}{\partial y}\Big)_{y=0}\,,$$
$$q_w = -k\Big(\frac{\partial T}{\partial y}\Big)_{y=0}, \quad j_w = -D_B\Big(\frac{\partial C}{\partial y}\Big)_{y=0}\,. \tag{13}$$

Dimensionless forms of Skin friction coefficient, the local Nusselt number, and the local Sherwood number are given by

$$C_f\mathrm{Re}_x^{1/2} = (1 + 3K)f''(0), \quad \mathrm{Nu}_x\mathrm{Re}_x^{-1/2} = -\theta'(0)\,,$$
$$\mathrm{Sh}\mathrm{Re}_x^{-1/2} = -\phi'(0)\,. \tag{14}$$

3 Homotopy Analysis Solutions

The velocity, temperature, and concentration distributions in form of base functions

$$\{\eta^k\exp(-n\eta)|k \geqslant 0, n \geqslant 0\}\,,$$

can be expressed as

$$f(\eta) = a_{0,0}^0 + \sum_{n=0}^{\infty}\sum_{k=0}^{\infty}a_{m,n}^k\eta^k\exp(-n\eta)\,, \tag{15}$$
$$\theta(\eta) = \sum_{n=0}^{\infty}\sum_{k=0}^{\infty}b_{m,n}^k\eta^k\exp(-n\eta)\,, \tag{16}$$
$$\phi(\eta) = \sum_{n=0}^{\infty}\sum_{k=0}^{\infty}c_{m,n}^k\eta^k\exp(-n\eta)\,, \tag{17}$$

in which $a_{m,n}^k$, $b_{m,n}^k$, and $c_{m,n}^k$ are the coefficients. Initial guesses and auxiliary linear operators are given in the following manner:

$$f_0(\eta) = 1 - \exp(-\eta)\,, \tag{18}$$
$$\theta_0(\eta) = \exp(-\eta)\,, \tag{19}$$
$$\phi_0(\eta) = \exp(-\eta)\,, \tag{20}$$
$$L_f = \frac{\mathrm{d}^3f}{\mathrm{d}\eta^3} - \frac{\mathrm{d}f}{\mathrm{d}\eta}\,, \tag{21}$$
$$L_\theta = \frac{\mathrm{d}^2\theta}{\mathrm{d}\eta^2} - \theta\,, \tag{22}$$
$$L_\phi = \frac{\mathrm{d}^2\phi}{\mathrm{d}\eta^2} - \phi\,, \tag{23}$$

satisfying the following properties

$$L_f[C_1 + C_2\exp(\eta) + C_3\exp(-\eta)] = 0\,, \tag{24}$$
$$L_\theta[C_4\exp(\eta) + C_5\exp(-\eta)] = 0\,, \tag{25}$$
$$L_\phi[C_6\exp(\eta) + C_7\exp(-\eta)] = 0\,, \tag{26}$$

where C_i ($i = 1$–7) are the arbitrary constants.

3.1 *zeroth Order Deformation Problems*

If $p \in [0, 1]$ is an embedding parameter and $\hbar_f$, $\hbar_\theta$ and $\hbar_\phi$ represent the non-zero auxiliary parameters. The zeroth-order deformation problems are:

$$(1 - p)L_f[\hat{f}(\eta, p) - f_0(\eta)] = p\hbar_fN_f[\hat{f}(\eta, p), \hat{\theta}(\eta, p), \hat{\phi}(\eta, p)]\,, \tag{27}$$
$$(1 - p)L_\theta[\hat{\theta}(\eta, p) - \theta_0(\eta)] = p\hbar_\theta N_\theta[\hat{f}(\eta, p), \hat{\theta}(\eta, p), \hat{\phi}(\eta, p)]\,, \tag{28}$$
$$(1 - p)L_\phi[\hat{\phi}(\eta, p) - \phi_0(\eta)] = p\hbar_\phi N_\phi[\hat{f}(\eta, p), \hat{\theta}(\eta, p), \hat{\phi}(\eta, p)]\,, \tag{29}$$

$$\hat{f}(\eta; p)|_{\eta=0} = 0, \quad \frac{\partial\hat{f}(\eta; p)}{\partial\eta}\Big|_{\eta=0} = 1\,,$$

$$\frac{\partial \hat{f}(\eta;p)}{\partial \eta}\Big|_{\eta=\infty} = 0\,, \tag{30}$$

$$\hat{\theta}(\eta;p)|_{\eta=0} = 1, \quad \hat{\theta}(\eta;p)|_{\eta=\infty} = 0\,, \tag{31}$$

$$\hat{\phi}(\eta;p)|_{\eta=0} = 1, \quad \hat{\phi}(\eta;p)|_{\eta=\infty} = 0\,, \tag{32}$$

in which the nonlinear operators N_f, N_θ, and N_ϕ are

$$N_f[\hat{f}(\eta;p),\hat{\theta}(\eta;p),\hat{\phi}(\eta;p)] = \frac{\partial^3 \hat{f}(\eta,p)}{\partial \eta^3} + \hat{f}(\eta,p)\frac{\partial^2 \hat{f}(\eta,p)}{\partial \eta^2} - \Big(\frac{\partial \hat{f}(\eta,p}{\partial \eta}\Big)^2 - \gamma\frac{\partial \hat{f}(\eta,p)}{\partial \eta} - K\Big\{\hat{f}(\eta,p)\frac{\partial^4 \hat{f}(\eta,p)}{\partial \eta^4} - 2\frac{\partial \hat{f}(\eta,p)}{\partial \eta}\frac{\partial^4 \hat{f}(\eta,p)}{\partial \eta^4} + \Big(\frac{\partial^2 \hat{f}(\eta,p)}{\partial \eta^2}\Big)^2\Big\} + \lambda(\hat{\theta}(\eta,p) + N\hat{\phi}(\eta,p))\,, \tag{33}$$

$$N_\theta[\hat{f}(\eta;p),\hat{\theta}(\eta;p),\hat{\phi}(\eta;p)] = \frac{1}{\mathrm{Pr}}\frac{\partial^2 \hat{\theta}(\eta,p)}{\partial \eta^2} + \hat{f}(\eta,p)\frac{\partial \hat{\theta}(\eta,p)}{\partial \eta} - \frac{\partial \hat{f}(\eta,p)}{\partial \eta}\hat{\theta}(\eta,p) + \mathrm{Df}\frac{\partial^2 \hat{\phi}((\eta,p)}{\partial \eta^2} + \mathrm{Nb}\frac{\partial \hat{\theta}(\eta,p)}{\partial \eta}\frac{\partial \hat{\phi}(\eta,p)}{\partial \eta} + \mathrm{Nt}\Big(\frac{\partial \hat{\theta}(\eta,p)}{\partial \eta}\Big)^2, \tag{34}$$

$$N_\phi[\hat{f}(\eta;p),\hat{\theta}(\eta;p),\hat{\phi}(\eta;p)] = \frac{\partial^2 \hat{\phi}(\eta,p)}{\partial \eta} + \mathrm{PrLe}\Big(\hat{f}(\eta,p)\frac{\partial \hat{\phi}(\eta,p)}{\partial \eta} - \frac{\partial \hat{f}(\eta,p)}{\partial \eta}\hat{\phi}(\eta,p)\Big) + \mathrm{SrLe}\frac{\partial^2 \hat{\theta}(\eta,p)}{\partial \eta^2} + \frac{\mathrm{Nt}}{\mathrm{Nb}}\frac{\partial^2 \hat{\theta}(\eta,p)}{\partial \eta^2}\,. \tag{35}$$

For $p = 0$ and $p = 1$, we have

$$\hat{f}(\eta;0) = f_0(\eta), \quad \hat{f}(\eta;1) = f(\eta)\,, \tag{36}$$

$$\hat{\theta}(\eta;0) = \theta_0(\eta), \quad \hat{\theta}(\eta;1) = \theta(\eta)\,, \tag{37}$$

$$\hat{\phi}(\eta;0) = \phi_0(\eta), \quad \hat{\phi}(\eta;1) = \phi(\eta)\,. \tag{38}$$

Expanding $\hat{f}(\eta,p)$, $\hat{\theta}(\eta;p)$, and $\hat{\phi}(\eta;p)$ in Taylor's theorem with respect to an embedding parameter p, one has

$$\hat{f}(\eta;p) = f_0(\eta) + \sum_{m=1}^{\infty} f_m(\eta)p^m, \tag{39}$$

$$\hat{\theta}(\eta;p) = \theta_0(\eta) + \sum_{m=1}^{\infty} \theta_m(\eta)p^m, \tag{40}$$

$$\hat{\phi}(\eta;p) = \phi_0(\eta) + \sum_{m=1}^{\infty} \phi_m(\eta)p^m, \tag{41}$$

$$f_m(\eta) = \frac{1}{m!}\frac{\partial^m \hat{f}(\eta;p)}{\partial p^m}\Big|_{p=0}, \quad \theta_m(\eta) = \frac{1}{m!}\frac{\partial^m \hat{\theta}(\eta;p)}{\partial p^m}\Big|_{p=0}, \quad \phi_m(\eta) = \frac{1}{m!}\frac{\partial^m \hat{\phi}(\eta;p)}{\partial p^m}\Big|_{p=0}. \tag{42}$$

The convergence at $p = 1$ of Eqs. (39)–(41) depend on proper choice of auxiliary parameters, then we have

$$f(\eta) = f_0(\eta) + \sum_{m=1}^{\infty} f_m(\eta)\,, \tag{43}$$

$$\theta(\eta) = \theta_0(\eta) + \sum_{m=1}^{\infty} \theta_m(\eta)\,, \tag{44}$$

$$\phi(\eta) = \phi_0(\eta) + \sum_{m=1}^{\infty} \phi_m(\eta)\,. \tag{45}$$

3.2 *m-th Order Deformation Problems*

The m-th order deformation problems are of the form

$$L_f[f_m(\eta,p) - \chi_m f_{m-1}(\eta)] = \hbar_f R_m^f(\eta)\,, \tag{46}$$

$$L_\theta[\theta_m(\eta,p) - \chi_m \theta_{m-1}(\eta)] = \hbar_\theta R_m^\theta(\eta)\,, \tag{47}$$

$$L_\phi[\phi_m(\eta,p) - \chi_m \phi_{m-1}(\eta)] = \hbar_\phi R_m^\phi(\eta)\,, \tag{48}$$

with boundary conditions

$$f_m(0) = f_m'(0) = f_m'(\infty) = 0\,, \tag{49}$$

$$\theta_m(0) = \theta_m(\infty) = 0\,, \tag{50}$$

$$\phi_m(0) = \phi_m(\infty) = 0\,, \tag{51}$$

$$R_m^f(\eta) = f_{m-1}''' - \gamma f_{m-1}' + \sum_{k=0}^{m-1}[f_{m-1-k}f_k'' - f_{m-1-k}'f_k' - K\{f_{m-1-k}f_k^{iv} - 2f_{m-1-k}'f_k''' + f_{m-1-k}''f_k''\}] + \lambda(\theta_{m-1} + N\phi_{m-1})\,, \tag{52}$$

$$R_m^\theta(\eta) = \frac{1}{\mathrm{Pr}}\theta_{m-1}'' + \sum_{k=0}^{m-1}[f_{m-1-k}\theta_k' - \theta_{m-1-k}f_k' + \mathrm{Nb}\theta_{m-1-k}'\phi_k' + \mathrm{Nt}\theta_{m-1-k}'\theta_k'] + \mathrm{Df}\phi_{m-1}'', \tag{53}$$

$$R_m^\phi(\eta) = \phi_{m-1}'' + \mathrm{PrLe}\sum_{k=0}^{m-1}[f_{m-1-k}\phi_k' - \phi_{m-1-k}f_k'] + \mathrm{SrLe}\theta_{m-1}'' + \frac{\mathrm{Nt}}{\mathrm{Nb}}\theta_{m-1}''\,, \tag{54}$$

$$\begin{cases} 0, & m \leqslant 1\,, \\ 1, & m > 1\,. \end{cases} \tag{55}$$

In the form of special solutions $f_m^*(\eta)$, $\theta_m^*(\eta)$, and $\phi_m^*(\eta)$, the general solutions are assumed to be

$$f_m(\eta) = f_m^*(\eta) + C_1 + C_2\exp(\eta) + C_3\exp(-\eta)\,, \tag{56}$$

$$\theta_m(\eta) = \theta_m^*(\eta) + C_4\exp(\eta) + C_5\exp(-\eta)\,, \tag{57}$$

$$\phi_m(\eta) = \phi_m^*(\eta) + C_6\exp(\eta) + C_7\exp(-\eta)\,. \tag{58}$$

Here, constants C_i ($i = 1$–7) through boundary conditions (49)–(51) are appended as

$$C_2 = C_4 = C_6 = 0, \quad C_3 = \Big|\frac{\partial f_m(\eta)}{\partial \eta}\Big|_{\eta=0}, \tag{59}$$

$$C_1 = -C_3 - f_m(0), \quad C_5 = -\theta_m(0), \\ C_7 = -\phi_m(0). \tag{60}$$

4 Optimal Convergence Control Parameters

Average squared residual errors suggested by Liao[31] have been employed to optimize values of auxiliary parameters $\hbar_f$, $\hbar_\theta$, and $\hbar_\phi$ by using the concept of minimization.

$$\epsilon_m^f = \frac{1}{k+1}\sum_{j=0}^{k}\Big[N_f\Big(\sum_{i=0}^{m}\hat{f}(\eta), \sum_{i=0}^{m}\hat{\theta}(\eta), \sum_{i=0}^{m}\hat{\phi}(\eta)\Big)_{\eta=j\delta\eta}\Big]^2 \cdot \mathrm{d}\eta, \tag{61}$$

$$\epsilon_m^\theta = \frac{1}{k+1}\sum_{j=0}^{k}\Big[N_\theta\Big(\sum_{i=0}^{m}\hat{f}(\eta), \sum_{i=0}^{m}\hat{\theta}(\eta), \sum_{i=0}^{m}\hat{\phi}(\eta)\Big)_{\eta=j\delta\eta}\Big]^2 \cdot \mathrm{d}\eta, \tag{62}$$

$$\epsilon_m^\phi = \frac{1}{k+1}\sum_{j=0}^{k}\Big[N_\phi\Big(\sum_{i=0}^{m}\hat{f}(\eta), \sum_{i=0}^{m}\hat{\theta}(\eta), \sum_{i=0}^{m}\hat{\phi}(\eta)\Big)_{\eta=j\delta\eta}\Big]^2 \cdot \mathrm{d}\eta, \tag{63}$$

where k in an integer. The total squared residual error is given by

$$\epsilon_m^t = \epsilon_m^f + \epsilon_m^\theta + \epsilon_m^\phi, \tag{64}$$

with $\delta\eta = 0.5$ and $k = 20$. These errors are minimized with the help of *Mathematica* BVPh 2.0. The optimal convergent control parameters at 3^{rd} order of approximations are $\hbar_f = -0.752\,93$, $\hbar_\theta = -0.907\,38$ and $\hbar_\phi = -0.933\,951$ with total averaged squared error $\epsilon_m^t = 0.000\,018\,021\,9$. Table 1 represents different averaged squared residual errors for $m = 3$ with $\gamma = \lambda = \text{Le} = \text{Pr} = 1$, $\text{Df} = 0.1$, $\text{Sr} = 0.2$, $\text{Nb} = 0.7$, $N = 0.5$ and $\text{Nt} = 0.1$. It is observed that averaged squared residual errors decrease for increasing higher order approximations. Figure 1 is plotted to depict the behavior of average squared residual error $\text{Co} = (\hbar_f = \hbar_\theta = \hbar_\phi)$ against one optimal value of all three auxiliary control parameters $\hbar_f, \hbar_\theta$ and $\hbar_\phi$ at $2^{\text{nd}}, 6^{\text{th}}$ and 10^{th} iterations using *Mathematica* package BVPh 2.0. It is found that as we increase the order of iteration the corresponding value of the optimal convergence control parameter is converging to -1.38 approximately.

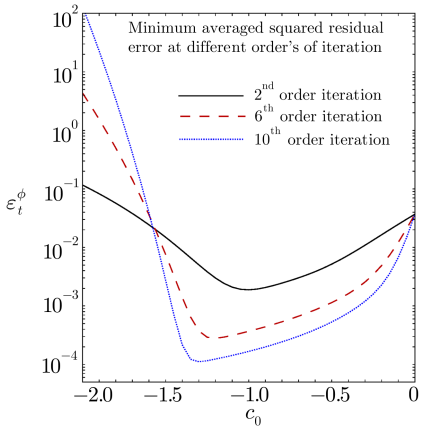

Fig. 1 Minimum averaged squared residual errors for $2^{\text{nd}}, 6^{\text{th}}$ and 10^{th} order of approximations.

Table 1 Averaged squared residual errors for different order of approximations.

m	ϵ_m^f	ϵ_m^θ	ϵ_m^ϕ
2	2.31×10^{-5}	5.29×10^{-5}	1.09×10^{-4}
6	4.91×10^{-8}	7.32×10^{-8}	5.28×10^{-8}
10	1.06×10^{-9}	9.76×10^{-9}	2.34×10^{-8}
16	7.27×10^{-12}	4.02×10^{-11}	7.36×10^{-11}
20	6.21×10^{-14}	1.42×10^{-12}	3.82×10^{-12}
26	3.25×10^{-15}	2.51×10^{-14}	5.1×10^{-14}
30	1.74×10^{-16}	1.13×10^{-15}	2.08×10^{-15}

5 Results and Discussion

Figures 2–21 are sketched to understand the effects of different arising parameters on velocity, temperature, and concentration profiles. Tabulated numerical values of skin friction coefficient parameter, local Nusselt and Sherwood numbers are also depicted in Tables 2 and 3 for numerous involved parameters. Figures 2, 3, and 4 illustrate the impact of viscoelastic parameter K on the fluid motion and consequently on dispersion of temperature and concentration profiles through the sheet as the time passes. The graphs clearly show that increasing values of viscoelastic parameter aids fluid's motion that is further away from the stretching sheet and offers resistance to the motion of the liquid nearer to the surface. Higher values of second-grade parameter is responsible for fluid's faster flow because of deterioration in the heat transfer. That is why escalation in momentum boundary layer and decrease in thermal and concentration boundary layers are encountered. Effect of porosity parameter γ on velocity profile is depicted in Fig. 5. It is observed that velocity profile decreases against increasing values of porosity parameter. Smaller permeability parameter is due to higher porosity parameter, which causes reduction in fluid's velocity. The graphs of mixed convective parameter against velocity, temperature and concentration profiles are plotted in

Figs. 6–8. It is observed from Fig. 6 that higher values of mixed convective parameter give rise to velocity profile. It is because of the fact that larger values of mixed convection parameter relates to the higher thermal buoyancy force which is accountable in enrichment of the velocity profile and reduction in temperature and concentration profiles (Figs. 7 and 8).

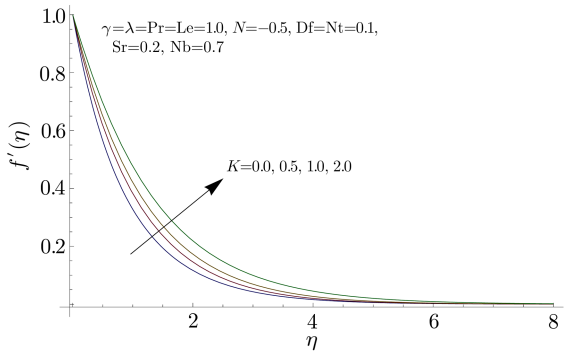

Fig. 2 Influence of K on $f'(\eta)$.

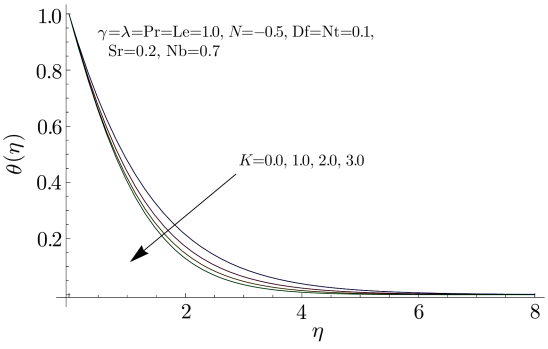

Fig. 3 Influence of K on $\theta(\eta)$.

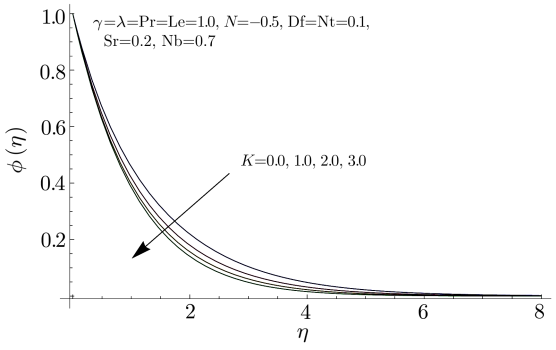

Fig. 4 Influence of K on $\phi(\eta)$.

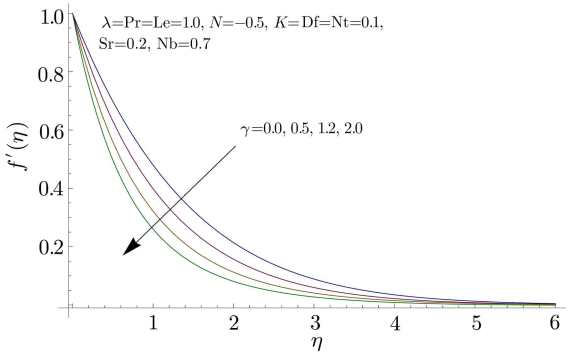

Fig. 5 Influence of γ on $f'(\eta)$.

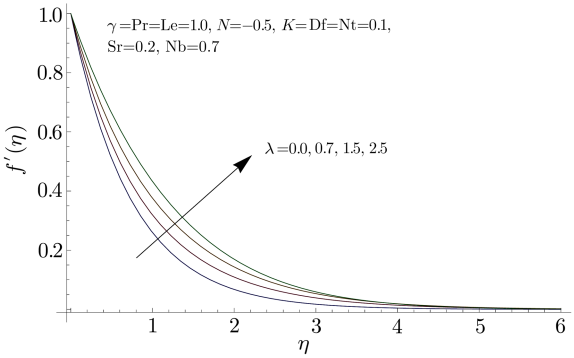

Fig. 6 Influence of λ on $f'(\eta)$.

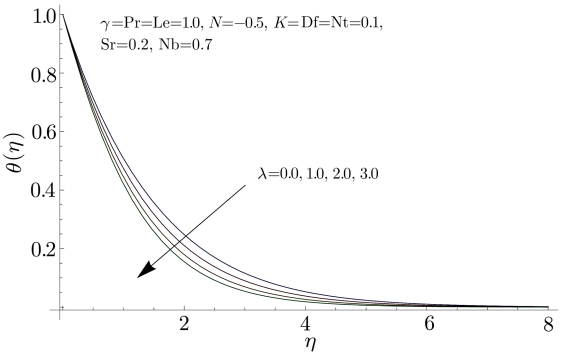

Fig. 7 Influence of λ on $\theta(\eta)$.

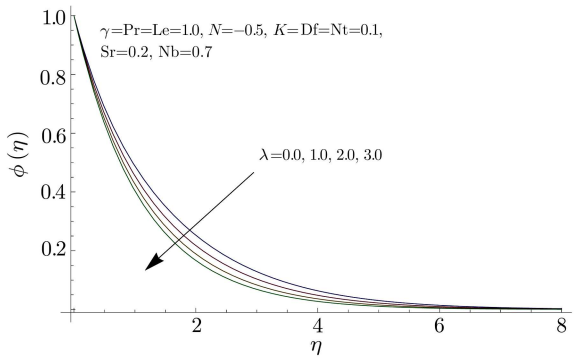

Fig. 8 Influence of λ on $\phi(\eta)$.

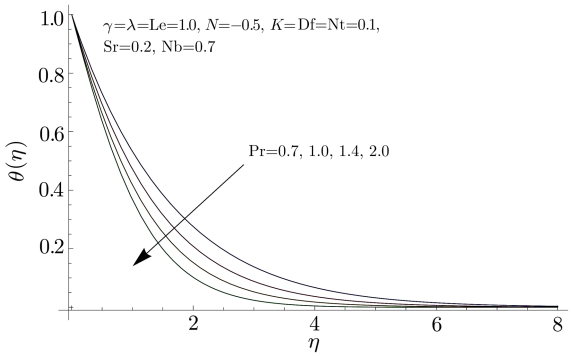

Fig. 9 Influence of Pr on $\theta(\eta)$.

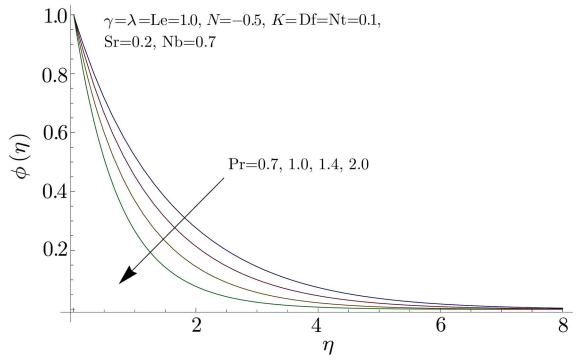

Fig. 10 Influence of Pr on $\phi(\eta)$.

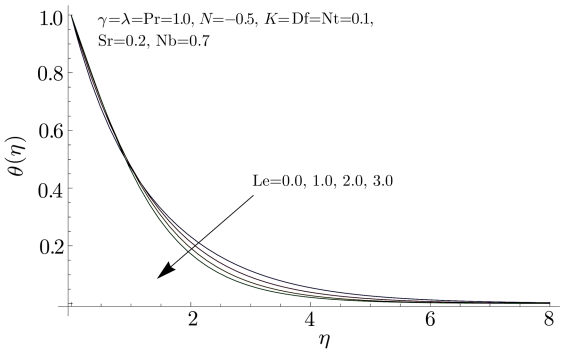

Fig. 11 Influence of Le on $\theta(\eta)$.

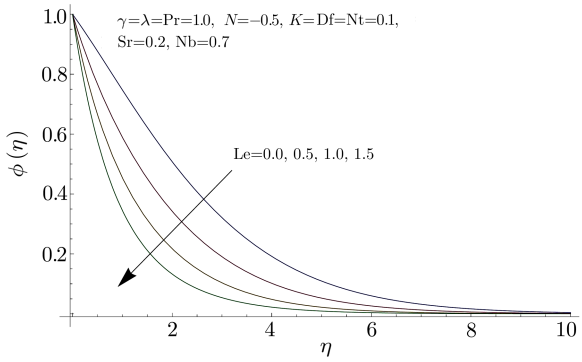

Fig. 12 Influence of Le on $\phi(\eta)$.

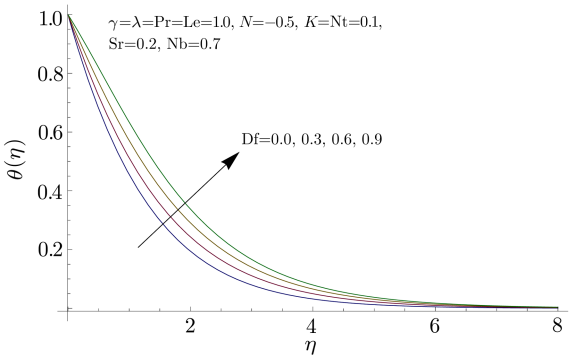

Fig. 13 Influence of Df on $\theta(\eta)$.

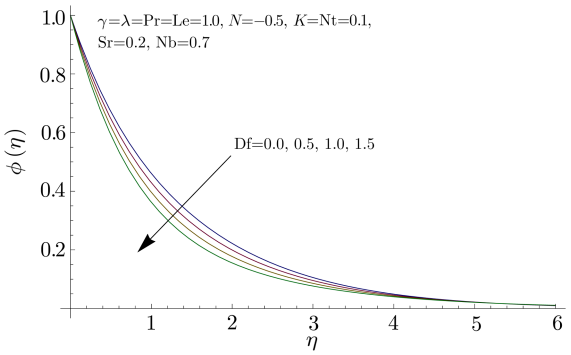

Fig. 14 Influence of Df on $\phi(\eta)$.

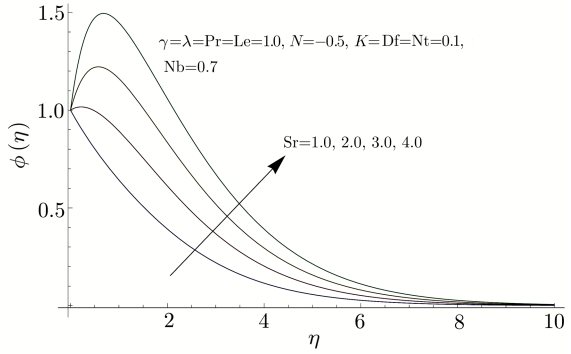

Fig. 15 Influence of Sr on $\phi(\eta)$.

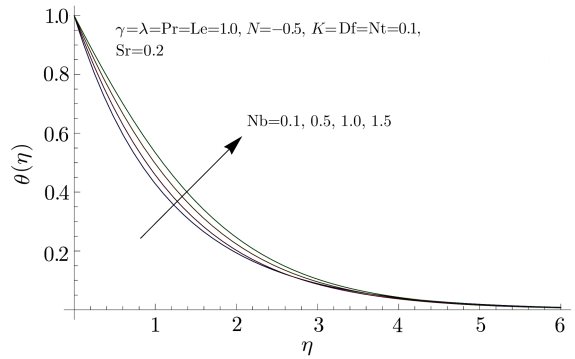

Fig. 16 Influence of Nb on $\theta(\eta)$.

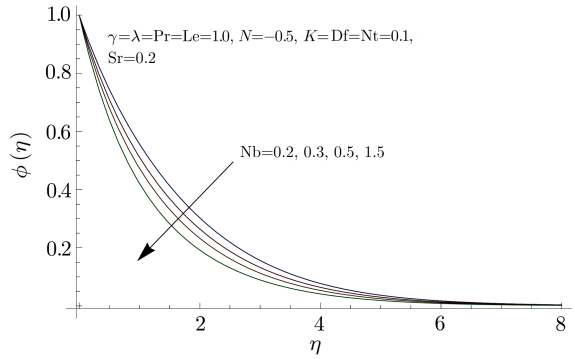

Fig. 17 Influence of Nb on $\phi(\eta)$.

Figures 9 and 10 are plotted to understand the effects of Prandtl number Pr on temperature and nanoparticle concentration fields. Thinner thermal and nanoparticle concentration boundary layer thickness are observed with increase in values of Prandtl number. Low thermal diffusivity is witnessed for higher Prandtl numbers which is main source for reedier thermal and nanoparticle concentration boundary layer thicknesses. Figures 11 and 12 are drawn to depict the effects of Lewis number Le on temperature and concentration fields respectively. For gradual increasing values of Lewis number, feeble molecular diffusivity and thinner boundary layer thickness is observed that eventually show decrease

in temperature and concentration fields. Influence of Dufour number on temperature and concentration profiles is depicted in Figs. 13 and 14.

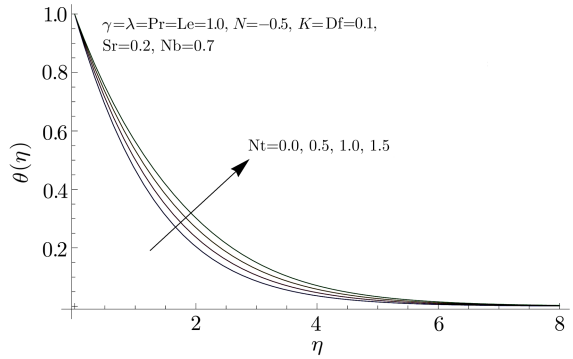

Fig. 18 Influence of Nt on $\theta(\eta)$.

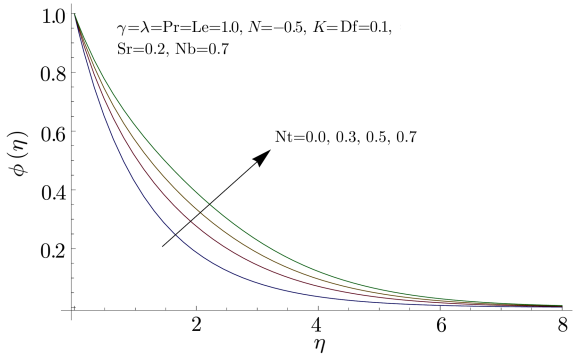

Fig. 19 Influence of Nt on $\phi(\eta)$.

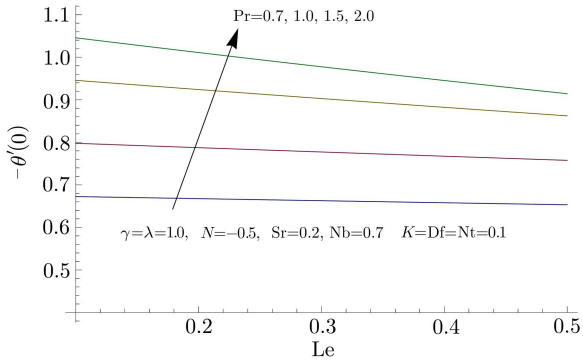

Fig. 20 Influence of Pr and Le on $-\theta'(0)$.

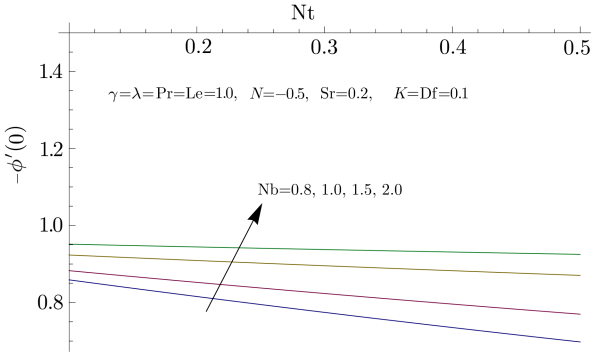

Fig. 21 Influence of Nb and Nt on $-\phi'(0)$.

Table 2 Values of the skin friction coefficient $C_f\mathrm{Re}_x^{1/2}$, local Nusselt number $\mathrm{Nu}_x\mathrm{Re}_x^{-1/2}$ and the local Sherwood number $\mathrm{Sh}\mathrm{Re}_x^{-1/2}$ for some values of K, γ, λ, N and Pr when Le = 1.0, Sr = 0.2, Nb = 0.7, Df = Nt = 0.1.

K	γ	λ	N	Pr	$-C_f\mathrm{Re}_x^{1/2}$	$-\mathrm{Nu}_x\mathrm{Re}_x^{-1/2}$	$-\mathrm{Sh}\mathrm{Re}_x^{-1/2}$
0.1	1.0	1.0	−0.2	1.0	1.299 15	0.730 67	0.865 86
0.0					1.042 09	0.725 51	0.857 85
0.2					1.541 81	0.735 16	0.872 95
0.4					1.994 53	0.742 71	0.885 16
	0.0				0.767 65	0.784 37	0.951 83
	0.5				1.051 34	0.755 98	0.906 75
	1.5				1.520 96	0.708 02	0.830 07
		0.0			1.752 92	0.667 93	0.759 83
		0.5			1.513 80	0.705 14	0.824 00
		1.2			1.217 63	0.739 27	0.879 65
			−0.5		1.454 97	0.712 18	0.835 02
			0.0		1.200 17	0.741 24	0.883 08
			0.5		0.965 54	0.763 66	0.919 19
				0.7	1.270 35	0.654 37	0.679 26
				1.2	1.312 18	0.758 85	0.982 49
				1.5	1.326 21	0.776 65	1.148 38

A gradual growth in temperature distribution is seen with increasing values of Dufour number. However, an opposite behavior is noticed in case of concentration profile. Effect of Soret number Sr on nanoparticle concentration field is illustrated in Fig. 15. It is observed that Soret number has a steadier and abetting effect on the concentration profiles throughout the boundary layer regime. With increase in Brownian motion parameter Nb, added heat will be generated due random motion of fluid particles which causes increase in temperature profile. This influence is portrayed

in Fig. 16. Effect of Brownian motion parameter Nb on concentration field is shown in Fig. 17. It is observed that increasing values Brownian motion parameter Nb results in escalation in random motion and collision of the macroscopic particles and eventually a decrease in fluid's concentration. Figures 18 and 19 are sketched to inspect the variation in the temperature and nanoparticle concentration for gradual increasing values of thermophoresis parameter Nt. The larger values of thermophoresis parameter result in high thermal and nanoparticle concentration boundary layer thicknesses. Figures 20 displays the behavior of Pr and Le on local Nusselt number. It is examined that local Nusselt number increases for larger values of Pr while decreases with increase in Le. Characteristics of Nb and Nt on local Sherwood number are demonstrated in Fig. 21. Local Sherwood number increases for larger values of Nb and decreases for higher values of Nt.

Table 3 Values of the skin friction coefficient $C_f\mathrm{Re}_x^{1/2}$, local Nusselt number $\mathrm{Nu}_x\mathrm{Re}_x^{-1/2}$ and the local Sherwood number $\mathrm{Sh}\mathrm{Re}_x^{-1/2}$ for some values of Sr, Df, Le, Nb, Nt when $K = 0.1$, $\gamma = \lambda = \mathrm{Pr} = 1.0$, $N = -0.5$.

Le	Df	Sr	Nb	Nt	$-C_f\mathrm{Re}_x^{1/2}$	$-\mathrm{Nu}_x\mathrm{Re}_x^{-1/2}$	$-\mathrm{Sh}\mathrm{Re}_x^{-1/2}$
0.7	0.1	0.2	0.7	0.1	1.316 66	0.769 10	0.655 31
1.2					1.290 95	0.709 87	0.988 80
1.5					1.281 74	0.683 39	1.154 09
	0.2				1.285 38	0.687 16	0.883 01
	0.3				1.271 64	0.641 70	0.900 33
	0.5				1.244 09	0.544 82	0.93 617
		0.0			1.291 30	0.714 55	0.952 76
		0.3			1.303 12	0.739 22	0.819 85
		0.5			1.311 33	0.757 36	0.722 15
			0.3		1.328 10	0.843 88	0.726 48
			0.5		1.312 02	0.884 51	0.820 12
			1.0		1.281 93	0.957 02	0.907 09
				0.3	1.299 62	0.709 13	0.757 32
				0.5	1.299 93	0.688 90	0.656 24
				0.7	1.300 11	0.669 95	0.561 71

Tables 2 and 3 display the numerical values of skin friction, local Nusselt, and local Sherwood numbers. It is witnessed that skin friction coefficient grows for higher values of K, γ, Pr, Sr, and Nt. Nevertheless, it decreases when values of λ, N, Le, Df and Nb. Local Nusselt number increases for increasing values of K, λ, N, Pr, Sr and Nb and decreases for increasing values of γ, Le, Df and Nt. It is also found that sherwood number increasing for larger values of K, λ, N, Pr, Le, Df and Nb and decreasing for higher values of γ, Sr and Nt.

6 Conclusion

Optimal solutions has been obtained for the boundary layer flow of viscoelastic nanofluid about a stretching vertical surface affected by Brownian and thermophoresis motions in the presence of mixed convection and Soret and Dufour effects past a porous media. A suitable similarity transformation is used to convert the momentum and the energy and concentration equations into a set of ordinary differential equations, which are solved by using Homotopy Analysis method. Salient features of presented investigation are:

- The nanofluid velocity increases with increase in mixed convective and viscoelastic parameters but it decreases with the increasing values of porosity parameter.
- Prandtl and Lewis numbers have similar effects on temperature and concentration profiles.
- Local Sherwood number decreases for higher values of thermophoresis parameter and increases for higher values of Brownian motion parameter.
- Brownian motion parameter has opposite influence on temperature and concentration profiles but similar effect is observed in case of thermophoresis parameter.
- Soret and Dufour numbers have opposite effect on concentration profile.
- Local Nusselt number increases for higher values of Prandtl number whereas it decreases with increase in values of Lewis number.
- Dufour number has opposite behavior on temperature and concentration profiles.

References

[1] D.B. Ingham and I. Pop, editors. *Transport Phenomena in Porous Media, vol. III*, Pergamon, Oxford (2005).

[2] D.A. Nield and A. Bejan, *Convection in Porous Media*, 3rd ed., Springer, New York (2006).

[3] I. Pop and D.B. Ingham, *Convective Heat Transfer: Mathematical and Computational Modeling of Viscous Fluids and Porous Media*, Pergamon, Oxford (2001).

[4] A. Bejan, I. Dincer, S. Lorente,*et al.*, *Porous and Complex Flow Structures in Modern Technologies*, Springer, New York (2004).

[5] K. Vafai, editor. *Handbook of Porous Media*, Taylor & Francis, New York (2005).

[6] P. Vadasz, *Bejan Aor. Emerging Topics in Heat and Mass Transfer in Porous Media*, ed. D.A. Nield, Springer, New York (2008).

[7] J.D. Jasen, *A Systems Description of Flow Through Porous Media*, Springer, Verlag (2013).

[8] A. Postelnicu, Int. J. Heat Mass Transfer **47** (2004) 1467.

[9] E.R. Eckert and R.M. Drake, *Analysis of Heat and Mass Transfer*, McGraw Hill, New York (1972).

[10] J.K. Platten and J.C. Legros, *Convection in Liquids*, Springer, New York (1984).

[11] A. Mojtabi and M.C. Charrier-Mojtabi, *Double-Diffusive Convection in Porous Media*, in: Vafai K, editor. *Handbook of Porous Media*, Marcel Dekker, New York (2000).

[12] M. Ramzan, M. Farooq, and T. Hayat, J. Cent. South Univ. **22** (2015) 707.

[13] T. Hayat, M. Bilal, A. Alsaedi, and M.S. Alhothuali, Int. J. Numer. Method H **25** (2105) 98.

[14] M. Ramzan and F. Yousaf, AIP Adv. **5** (2015) 057132.

[15] T. Hussain, S.A. Shehzad, T. Hayat, *et al.*, Plos One **9** (2014) e103719.

[16] O.D. Makinde and A. Aziz, Int. J. Therm. Sci. **50** (2011) 1326.

[17] A. Malvandi, T. Hedayati, and D.D. Ganji, Powder Technol. **253** (2014) 377.

[18] R. Cortell, Energy **74** (2014) 377.

[19] M. Ramzan and M. Bilal, Plos One **10** (2015) e0122929.

[20] T. Hayat, T. Muhammad, S.A. Shehzad, and A. Alsaedi, Int. J. Numer. Method H **25** (2014) 762.

[21] S.U.S. Choi, Proceeding of ASME Int. Mech. Engg. Congr. Expo. **66** (1995) 99.

[22] A. Mushtaq, M. Mustafa, T. Hayat, and A. Alsaedi, Int. J. Nonlin. Mech. **79** (2016) 83.

[23] M. Ramzan and M. Bilal, J. Mol. Liq. **215** (2016) 212.

[24] R. Dhanai, R. Rana, and L. Kumar, Powder Technol. **288** (2016) 140.

[25] M. Sheikholeslami and D.D. Ganji, Powder Technol. **253** (2014) 789.

[26] M. Ramzan, S. Inam, and S.A. Shehzad, Alexand. Eng. J. **55** (2016) 311.

[27] M. Ramzan, Plos One **10(4)** (2015) e0124699.

[28] F. Hedayati and F. Domairry, Powder Technol. **272** (2015) 250.

[29] A.K. Gupta and S. Ray, Powder Technol. **279** (2015) 282.

[30] S.J. Liao, Commun. Nonlinear Sci. **15** (2010) 2003.

[31] T. Hayat, T. Muhammad, S.A. Shehzad, and A. Alsaedi, Adv. Powder Technol. **27** (2016) 504.

[32] U. Farooq, Y.L. Zhao, T. Hayat, A. Alsaedi, and S.J. Liao, Comput. Fluids **111** (2015) 69.

[33] S. Nadeem, S. Masood, R. Mehmood, and M.A. Sadiq, Plos One **10** (2015) e0124016.

[34] M.M. Rashidi, S. Bagheri, E. Momoniat, and N. Freidoonimehr, Ain Shams Eng. J. (2015), doi:10.1016/-j.asej.2015.08.012.